

#### **CFD** Letters



Journal homepage: https://semarakilmu.com.my/journals/index.php/CFD\_Letters/index ISSN: 2180-1363

# Study of Airflow Dynamics and Particle Transport in the Upper Respiratory System using Numerical Simulation

Anirudh Krishna Mittal<sup>1</sup>, John Valerian Corda<sup>2</sup>, Kevin Amith Mathias<sup>1</sup>, Shah Mohammed Abdul Khader<sup>1</sup>, Augustine B.V. Barboza<sup>1</sup>, Kamarul Arifin Ahmad<sup>3</sup>, Mohammad Zuber<sup>2</sup>, Gowrava Shenoy<sup>1,\*</sup>

- Department of Mechanical & Industrial Engineering, Manipal Institute of Technology, Manipal Academy of Higher Education, Manipal 576104, Karnataka, India
- Department of Aeronautical & Automobile Engineering, Manipal Institute of Technology, Manipal Academy of Higher Education, Manipal 576104. Karnataka. India
- Department of Aerospace Engineering, Faculty of Engineering, Universiti Putra Malaysia, 43400 Serdang, Selangor, Malaysia

#### **ARTICLE INFO**

# ABSTRACT

#### Article history:

Received 4 May 2024
Received in revised form 8 June 2024
Accepted 10 July 2024
Available online 31 December 2024

The increase in pollution levels in recent years has increased the prevalence of pulmonary diseases. The accumulation of pollutant particles in the pulmonary tract is speculated to be one of the major reasons for the increase in chronic cases. This necessitates the study of the mechanism of particle deposition in human airways to develop better drug delivery systems. Aerosolized forms of drugs are commonly used to treat pulmonary diseases. The current study employed computational fluid dynamics (CFD) and discrete element method (DEM) techniques to study airflow patterns and particle deposition phenomena. An idealized 3D CAD model was developed based on available literature. A discretized finite-volume model was tested to ensure an independent solution. A user-defined function (UDF) was used to simulate realistic breathing dynamics for the respiration cycle. The aerosol particles of the calculated volume were mixed into the airflow domain. The analysis was conducted using ANSYS FLUENT CFD solver. This study found several regions of high turbulence in the upper human airways, with secondary flow structures exhibiting bifurcations and the glottal region. The study also found that the oral cavity and oropharynx regions with higher turbulence intensity had a concentrated deposition of particles. Most of the aerosol particles (5µm) were transported into the alveolar sacs, where they were absorbed into the bloodstream. The oral cavity and oropharynx have the highest pressure and particle deposition efficiency, while the trachea plays a crucial role in particle deposition during inhalation due to weak oscillatory flows and turbulence, especially in the tracheal region and lower respiratory tract. The oral cavity has the highest efficiency at 7.32%, while the trachea has the lowest at 0.4%. The overall deposition efficiency across all regions is 9.078%. This study did not account for the breakup of aerosol particles. Aerosol particles can break apart due to airflow and collisions, affecting their size and deposition efficiency. Ignoring this breakup could lead to inaccurate results, making accurate dosimetry essential for inhalation studies.

#### Keywords:

Human airway; CFD; Discrete Element Method; aerosol simulation

E-mail address: gowrav.shenoy@manipal.edu (Gowrava Shenoy)

https://doi.org/10.37934/cfdl.17.6.171188

<sup>\*</sup> Corresponding author.

#### 1. Introduction

The recent surge in interest among researchers studying particle transport in human airways has mostly focused on addressing concerns about air pollution and its harmful impact on public health. The World Health Organization (WHO) reports that 90% of people worldwide breathe polluted air, resulting in approximately 8 million deaths per year, with outdoor pollution causing 4.2 million deaths and indoor pollution causing 3.8 million deaths [1]. Nearly half of these deaths result from lung diseases, including about a tenth from lung cancer, a fifth each from chronic obstructive pulmonary disease and pneumonia [2]. With increasing population densities and mass migration to urban areas, air pollution has become a significant problem. On average, people living in dense urban areas are at a much higher risk of developing chronic lung diseases such as emphysema and COPD, without a genetic predisposition to them. In response to this growing problem, the study of particle deposition in human airways has taken the front seat of the biomechanics community. Gaining insight into airflow dynamics during respiration is crucial for analysing the deposition behaviour of particles within the lungs. Air movement through the human airway is a complex phenomenon that exhibits areas of separated flow and development of recirculatory regions [3,4].

Computational fluid dynamics is a method that allows for the numerical calculation of flow field parameters and arrives at an approximate solution [5,6]. The first step to conducting a CFD analysis of airflow patterns and particle transport in the lungs involves creating a morphological model of the respiratory tract. The most used scheme for describing the human airways shown in Figure 1 is Weibel's scheme, which involves assigning numerical values to the branching sections of the lungs, referred to as generations. The scheme starts from the trachea, is assigned as generation 0 and progresses sequentially until the final alveolar sacs, which are nomenclature as generation 23. Research conducted by Napoli *et al.*, [7] shows that the WoB model bases itself on the assumption that breathing is sinusoidal.

Current studies that use CFD models to simulate particle transport in human airways simulate fully developed flows. However, respiration is a complex transient phenomenon that exhibits significant changes in the flow characteristics in the areas of flow separation and the development of secondary flow [3,4]. These flow phenomena had a significant impact on the particle deposition pattern. Therefore, this study used instantaneous flow rate data during respiration to gain a better understanding [8]. Current research in the field is primarily focused on investigating particle transport phenomena under steady-state conditions by utilizing idealized sinusoidal breathing curves and geometrically symmetric models of the bronchial tree. In this study, a realistic breathing curve and an asymmetric idealized geometry were considered to provide further insights into particle transport dynamics. This will aid in the development of more effective aerosolized drug delivery systems. A new numerical model studies particle deposition in terminal bronchioles. Larger particles deposit at bifurcation areas, smaller ones at walls. Right lung shows higher deposition efficiency. Results can help optimize drug delivery in targeted airways [9]. A study simulated expiratory airflow in a respiratory tract model. Turbulence was highest in the mouth-pharynx region, influenced by expiration and glottis motion. Neglecting these factors significantly altered airflow characteristics, emphasizing the importance of clinically informed modelling [10]. Middle Turbinectomy (MT) alters nasal anatomy and airflow, affecting pollen inhalation. Six Functional Endoscopic Sinus Surgery (FESS) models underwent MT simulations, which escalated airflow in upper-middle nasal region. MT type affected deposition patterns, especially for particles <50 μm. Findings inform post-MT pollen exposure risk assessments [11].

The study of airway bifurcations has proven challenging; however, computational fluid dynamics (CFD) is a viable method for assessing the effectiveness of pharmaceutical aerosols in treating

respiratory disorders. The Computational Fluid Dynamics (CFD)—Discrete Element Method (DEM) approach can accurately simulate the behaviour of gas-solid flow with strong coupling, as well as the motion of non-spherical particles, by considering factors such as particle-particle collision and particle rotation, as well as the volume of particles in the fluid [12]. Therefore, this approach has great potential for simulating the transport and deposition of fibrous particles in alveolar regions. The CFD-DEM was used to study the subject matter in question. This study employed a three-dimensional model with four ramifications to investigate particle deposition. The novel contribution of this study includes the investigation of particle transport dynamics in human airways using realistic breathing curves and asymmetric geometries. By integrating Computational Fluid Dynamics (CFD) with the Discrete Element Method (DEM), the research addresses air pollution's impact on respiratory health [13,14]. It also optimizes pharmaceutical aerosol delivery systems and the mechanisms of particle deposition in alveolar regions.

Steady-state models may not consider the impact of changes in breathing patterns on aerosol particle size and distribution. For example, deep breaths can enhance particle deposition, while slower breathing may reduce it for smaller particles. This study uses more realistic breathing patterns to understand how aerosols behave in the respiratory tract. It helps assess particle deposition efficiency and potential health impacts, especially for vulnerable populations. This research provides insights for improving dosimetry and risk assessment in inhalation studies, enhancing our understanding of aerosol dynamics in human health.

## 2. Methodology

## 2.1 Geometry Development

Based on the dimensions from the literature [15], an anatomically representative idealized geometry model was created using Fusion 360 software. The idealized geometry consisted of the opening of the mouth (modelled as a circular opening of  $\emptyset$ 20 mm) oral cavity, soft palate oropharynx and glottis. The lower respiratory tract model is based on the findings of Weibel [8]. Weibel's scheme which is a numerical classification system used to describe the branching structure of the lungs, which are divided into generations starting from the trachea, labelled as 0 and continuing down to the alveolar ramifications. Weibel also provided branching ratios and aspect ratios of the bronchial tree. The angle of divergence is obtained from Horsfield  $et\ al.$ , [16] . Figure 1 shows the upper and lower respiratory tract and the various other parameters used.

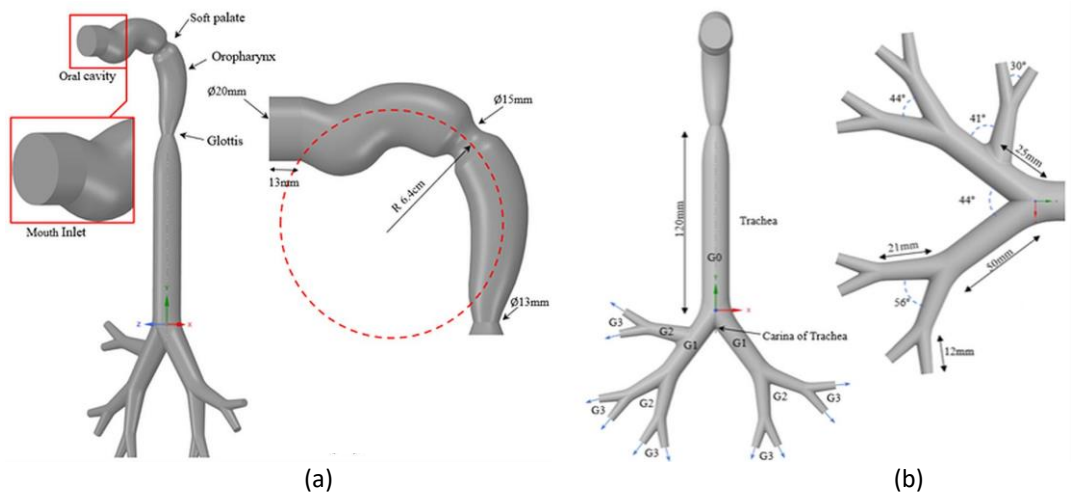


**Fig. 1.** Idealised model and general dimensions of (a) upper respiratory tract (b) lower respiratory tract

#### 2.2 Mesh Generation

Tetrahedral elements ranging from 1 mm to 0.5 mm were used to create the final mesh. The inclusion of a boundary layer mesh was crucial to determine the appropriate first cell height and total thickness of the inflation mesh and the Y+ parameters were considered by Augusto *et al.*, [17].

$$Y += \frac{\mu_{\tau} \cdot \Delta y_1 \cdot \rho}{\mu} \tag{1}$$

In Eq. (1),  $u_{\tau}$  is the friction velocity,  $\Delta y_1$  is the distance between the first cell centre and the wall, p is the density of the fluid and  $\mu$  is the viscosity of the fluid. Given the utilization of a k- $\Omega$  SST model, the Y+ values were maintained below 10. This ensured that the mesh resolved the flow near the wall more accurately, leading to more reliable predictions and simulations. In the presence of turbulent flow, there are notable changes in velocity near the respiratory wall. This highlights the importance of choosing the right y-plus (y+) values to ensure accurate prediction of wall-bounded flow using turbulence models. Proper selection of y-plus values is critical to capture these complex flow dynamics and obtain precise simulation results, especially when dealing with turbulent airflow in the respiratory tract [18]. In simulations of turbulent flows, like those in the respiratory system, the yplus value helps determine the appropriate turbulence modelling approach. By selecting the correct y-plus values, researchers can ensure that their simulations accurately reflect physical processes in the respiratory tract, such as particle deposition and airflow patterns, essential for developing effective inhalation therapies and understanding the behaviour of aerosolized drugs in the lungs' complex architecture. By substituting these values, we obtain Δy<sub>1</sub> as 6.43. A grid independence study was conducted to ensure that the results were independent of the grid size. Five different steadystate analyses were performed with grid sizes of 2, 1.5, 1, 0.5 and 0.25 mm. The mean velocity values through the four planes were calculated and the results are shown in Figure 2.

As shown in Figure 2(b), the change in the velocity magnitude becomes negligible at 509,172 elements for planes 1-1' and 2-2', which corresponds to an element size of 1mm. Similarly, the velocity magnitude remained relatively unchanged at planes 3-3' and 4-4' after 2,395,592 elements, corresponding to an element size of 0.5mm.

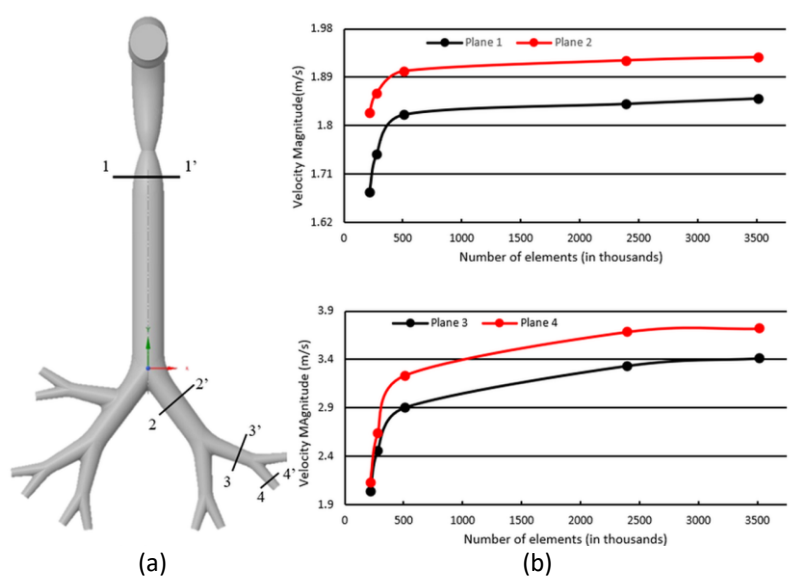


**Fig. 2.** Graphic depicting (a) location of probe planes (b) mean velocity magnitudes

The final grid was created based on the findings of a grid independence study that utilized multiple element sizes. Coarser sizes were assigned to areas exhibiting grid independence, whereas finer sizes were assigned to more sensitive regions. The final mesh contained 2.8 million nodes and 1.3 million elements. The quality statistics of the meshes are listed in Table 1.

**Table 1**Mesh quality statistics

iviesii quanty statistics				
Property	Max	Min	Average	
Element Quality	0.9999	5.1319x10 <sup>-2</sup>	0.4232	
Aspect Ratio	34.8780	1.7121	7.7196	
Skewness	0.7835	6.2055x10-4	0.2012	
Orthogonal Quality	0.9925	0.2166	0.7983	

A user-defined function (UDF) is a user-defined program that can be dynamically loaded with the ANSYS FLUENT solver to enhance its standard features. In this study, UDFs were used to apply a variable Mass Flow Inlet boundary condition based on the data collected from Larrabee *et al.*, [19] and Zechman *et al.*, [20]. The transient volumetric flow rate of respiration available in the literature [19] was initially digitized using Origin graphing software. Figure 3(a) shows the ideal breathing curve and Figure 3(b) shows the curve obtained from the data points extracted. The data points were at interval of 0.08s. As can be seen from the graph, the inhalation period lasts for 2.28 seconds and exhalation lasted for 3.451 s. The total respiration cycle lasts for 5.71s. It can also be observed that the graph is not sinusoidal and the rate at which inhalation proceeds is slightly higher than that of respiration.

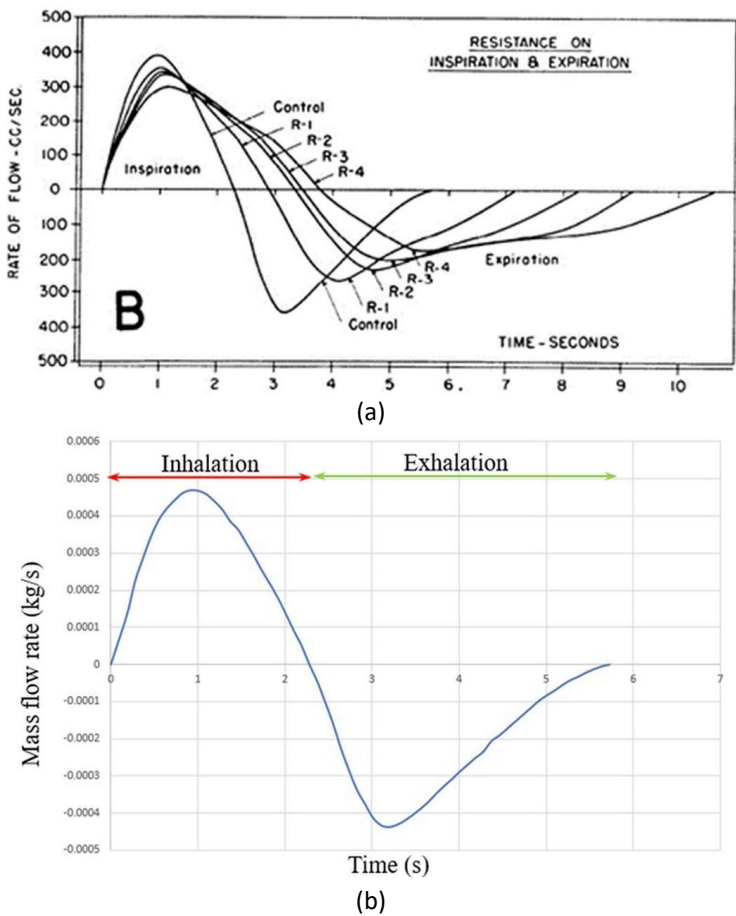


**Fig. 3.** Breathing curves with graded resistance and Breathing Curve with extracted data points [15]

Because the data are periodic, a Fourier series expansion (FSE) is obtained through MATLAB's inbuilt curve-fitting function. FSE simulates the periodic nature of human breathing and enables us to simulate multiple breathing cycles. Table 2 lists the Fourier coefficients used and Eq. (2) is the function that was imported into the FLUENT solver.

$$f(x) = a_0 + a_1 \sin(x \cdot \omega) + b_1 \cos(x \cdot \omega) + a_2 \sin(2x \cdot \omega) \dots + b_n \cos(nx \cdot \omega)$$
 (2)

Eq. (3) and Eq. (4) (along with the energy equation) form the Navier Stokes equations. These equations can be solved numerically to solve 3D gas flow. The Reynolds Numbers for each bifurcation were calculated by considering the diameter of each bifurcation. The calculated Reynolds numbers ranged from 2600 to 3700. These values indicated the need to use Turbulence models. In accordance with this, the SST (Shear stress transport)  $k-\Omega$  model was employed to capture the low Re turbulent nature of airflow [17,21].

**Table 2**Fourier coefficients

Tourier coefficients				
n	an	bn		
		_		
0	-1.487e-05	-		
1	2.199e-04	3.195e-04		
2	-1.112e-04	1.741e-05		
3	-1.796e-05	2.723e-05		
4	-3.169e-05	-8.517e-06		
5	-7.837e-06	3.338e-06		
6	-1.092e-05	-2.782e-06		
7	-5.628e-06	-5.918e-07		
8	-5.903e-06	-1.61e-06		

$$\nabla \cdot (\rho v^{\rightarrow}) = 0 \tag{3}$$

$$\nabla \cdot (\rho v^{\rightarrow} v^{\rightarrow}) = -\nabla p + \nabla \cdot (\mu (\nabla v^{\rightarrow} + \nabla v^{\rightarrow T})) + \rho g^{\rightarrow}$$
(4)

where  $\rho$  is the density of air,  $v^{\vec{}}$  is the velocity vector, p is the pressure,  $g^{\vec{}}$  is the gravitational force vector and  $\mu$  is the viscosity. These equations (along with the energy equation) form the Navier Stokes' equations.

The parameters of the fluid phase were chosen based on the normal human body temperature (310.15 K). The particle phase was defined based on the properties of the aerosolized drug formulation. This formulation is commonly used for treating COPD patients (Formoterol Fumerate Dihydrate IP and Budesonide IP) [22]. The trajectories of individual aerosolized particles were tracked using a Lagrangian approach. The volume flow rate of the particles injected in one actuation was  $7.598 \times 10^{-5}$  cc/s. Therefore, a one-way coupling was chosen to simulate the interaction between the particles and the air. The particle size of  $5 \mu m$  diameter was used [20,23]. The density of the particles was the same as that used in the formulation. The properties of the fluids and aerosols used in this study are listed in Table 3.

**Table 3**Discrete phase properties

2 13 of the printed properties			
Phase	Property	Value	
Fluid (air)	Viscosity	1.90 x 10-5 Pa s	
	Density	1.123 kg m-3	
Discrete Phase (Aerosol)	Diameter	5μm	
	Density	887 kg/m3	

The properties of the aerosol in Table 3 suggest that it is dense, possibly consisting of either liquid droplets, such as those found in aerosolized medications delivered via nebulizers or solid particulates, like dust, smoke or industrial emissions suspended in the air. The trajectories were tracked using a force balance that included the terms for gravity and drag. This relationship is as given in Eq. (5) and Eq. (6):

$$\frac{dv_p}{dt} = \frac{18\mu}{\rho_p d_p^2} \frac{C_D Re_p}{24} \left( v_p^{\rightarrow} - v^{\rightarrow} \right) + g^{\rightarrow} \left( \frac{\rho_p - \rho}{\rho_p} \right) \tag{5}$$

$$Re_p = \frac{\rho_f |v_p^{\rightarrow} - v_p| d_p}{\mu} \tag{6}$$

Here  $\overrightarrow{v_p}$ ,  $Re_p$  are the velocity vectors and dimensionless Reynolds number of the particles respectively. And  $C_D$  is the drag coefficient of the particle. In this case the particles are assumed to be perfectly spherical. Since the particles are above the micron range Brownian motion was neglected.

#### 2.3 Boundary Conditions

The inlet air flow profile at the mouth opening was described by using an UDF. The maximum flow rate at peak of inhalation was 23 L min<sup>-1</sup> [20]. A constant -98.665 Pa [24] relative pressure was adopted at the domain outlets (G3). This was done to simulate the negative intra-alveolar pressure that is generated when thoracic cavity expands due to the diaphragm contracting. Other studies have used an inflow boundary condition was applied at G0, while pressure outlet boundary conditions were specified at all terminal bronchi exits [25,26].

During the exhalation phase the inlet and outlet are reversed, that is, G3 becomes the inlet and the opening of the mouth becomes the outlet, all the above boundary conditions are kept constant with exception of now a +98.665 Pa relative pressure is applied at outlet. Table 4 and Table 5 better illustrate the boundary conditions used.

A fixed time step of 0.001s was used with a convergence criterion of the order 10<sup>-6</sup>. This time step size ensured that the courant number was of the order of unity. The Courant number, named after mathematician Richard Courant, is a dimensionless quantity. Numerically it can be defined in Eq. (7) as:

$$C = \sum_{i} \frac{U_i \Delta t}{\Delta h_i} \tag{7}$$

where  $U_i$  is the flow velocity,  $\Delta t$  is the time step size and  $\Delta h_i$  is the characteristic size of the mesh cell in the i direction. A maximum of 20 iterations were computed for every time step. The SIMPLE (Semi-Implicit Method for Pressure Linked Equations) coupling scheme was used for simulating fluid flow.

**Table 4**Boundary conditions during inhalation

Zone	Boundary Condition	Value
Inlet (mouth opening)	Mass Flow inlet	Defined by UDF
	DPM	Escape
Outlet (lower generations)	Pressure outlet	-98.665 Pa
	DPM	Escape
Wall (airway walls)	Fluid	No slip
	DPM	Trap

**Table 5**Boundary conditions during exhalation

	•	
Zone	<b>Boundary Condition</b>	Value
Inlet (lower generations)	Mass Flow inlet	Defined by UDF
	DPM	Escape
Outlet (mouth opening)	Pressure outlet	+98.665 Pa
	DPM	Escape
Wall (airway walls)	Fluid	No slip
	DPM	Trap

To accurately simulate the phases of inhalation and exhalation in the respiratory system, specific boundary conditions were established. A User-Defined Function (UDF) was utilized to create a realistic airflow by setting a mass flow inlet, paired with a pressure outlet of -98.665 Pa to mimic the intra-alveolar pressure, facilitating proper airflow into the alveoli. For the exhalation phase, the setup was adjusted: the mass flow inlet was positioned at the lower generations and the mouth opening served as the pressure outlet with a setting of +98.665 Pa to mirror the breathing process accurately. The effectiveness and accuracy of the UDF and boundary conditions were verified by comparing the simulation outcomes with data from well-recognized studies, ensuring the model's reliability and precision.

## 3. Results

#### 3.1 Pressure Distribution

Respiration in humans is a complex process primarily driven by pressure differentials. The contraction of the diaphragm and expansion of the thoracic cavity during inhalation create negative pressure in the alveolar sacs, known as intra-alveolar pressure (IAP). This negative pressure facilitates the intake of oxygen into the lungs, allowing efficient gas exchange. During various phases of respiration, the IAP undergoes changes, but it typically peaks at approximately 1 cm of the water head. Oral cavity and oropharynx regions exhibited the highest amount of mean pressure as shown in Figure 4.

The region after the glottis also showed a significant drop in pressure; this was present due to the sudden constriction in the throat region. The lowest negative pressure was observed right after the glottal region with a value of -122.127 Pa at peak inhalation and the highest value of pressure was observed in the oral cavity region with a value of -60.184 Pa.

The highest-pressure value of -60.184 Pa recorded in the oral cavity may contrast with some existing literature, which indicates that pressure in this area can be less negative due to the interplay of airflow dynamics and resistance in the oral cavity [27,28]. This discrepancy could stem from variations in study methodologies, including different modelling techniques or unique anatomical characteristics of the subjects. A more thorough comparison with established studies could offer further insights into these dynamics and improve our understanding of respiratory mechanics.

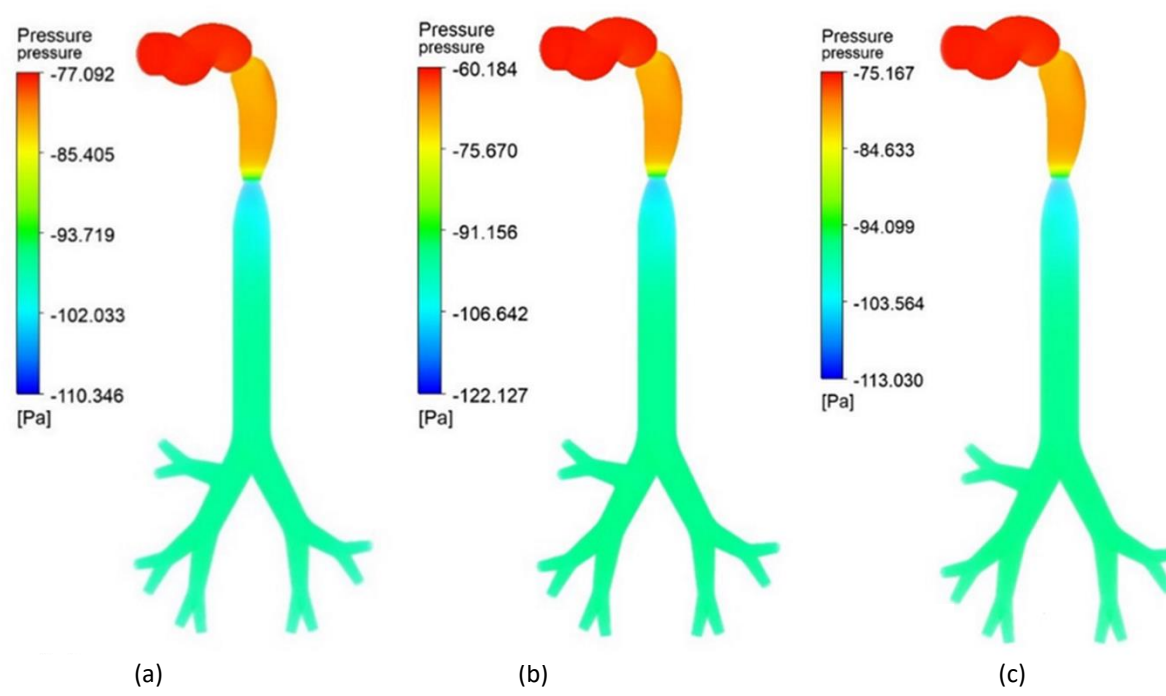


Fig. 4. Pressure contours in the human respiratory tract at (a) 0.45s (b) 0.99s (c) 1.45s

#### 3.2 Pressure Variation

The regional pressure variation is shown in Figure 5. As can be seen from the figure, the mouth and oropharynx region show the highest-pressure values. Another observation is that the pressure values in the upper regions of the airways are larger than in the lower airways. The average pressure remained relatively unchanged in the higher generations throughout the cycle. Any disruption in the pressure gradient within the respiratory tract can have adverse effects on normal breathing. If the pressure gradient is compromised, it can impede the flow of air in and out of the lungs, leading to breathing difficulties Understanding the importance of maintaining the appropriate pressure differentials in the respiratory system is crucial for diagnosing and managing respiratory disorders effectively.

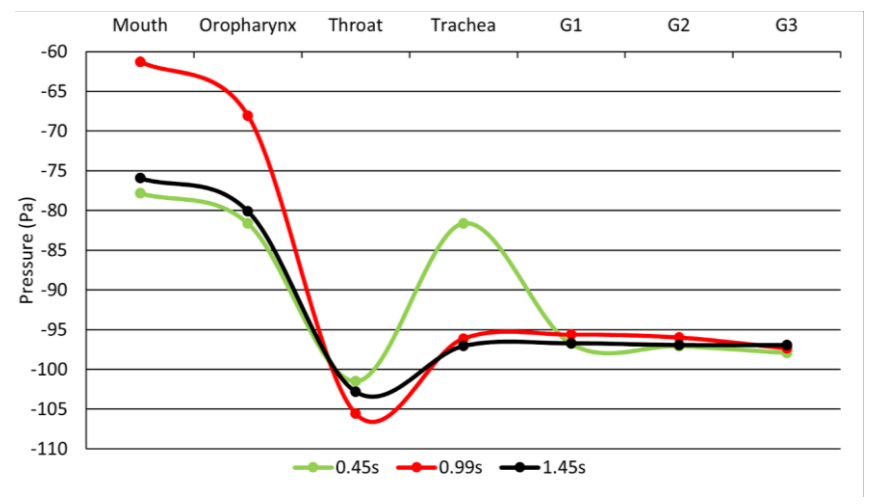


Fig. 5. Regional pressure variation

### 3.3 Velocity Analysis

## 3.3.1 Inhalation flow fields

The calculated velocity field at 0.917s (peak of inhalation) is shown in Figure 6. A strong axisymmetric flow can be observed within the trachea when viewed from the front; this is due to the sudden constriction in the throat region. The strength of this flow progressively increased as inhalation proceeded and subsequently diminished towards the end of the cycle. Additionally, the flow was concentrated towards the left side of the trachea. Vector plots on planes 1-1', 2-2', 3-3' and 4-4' are also shown the plots are from a top view perspective.

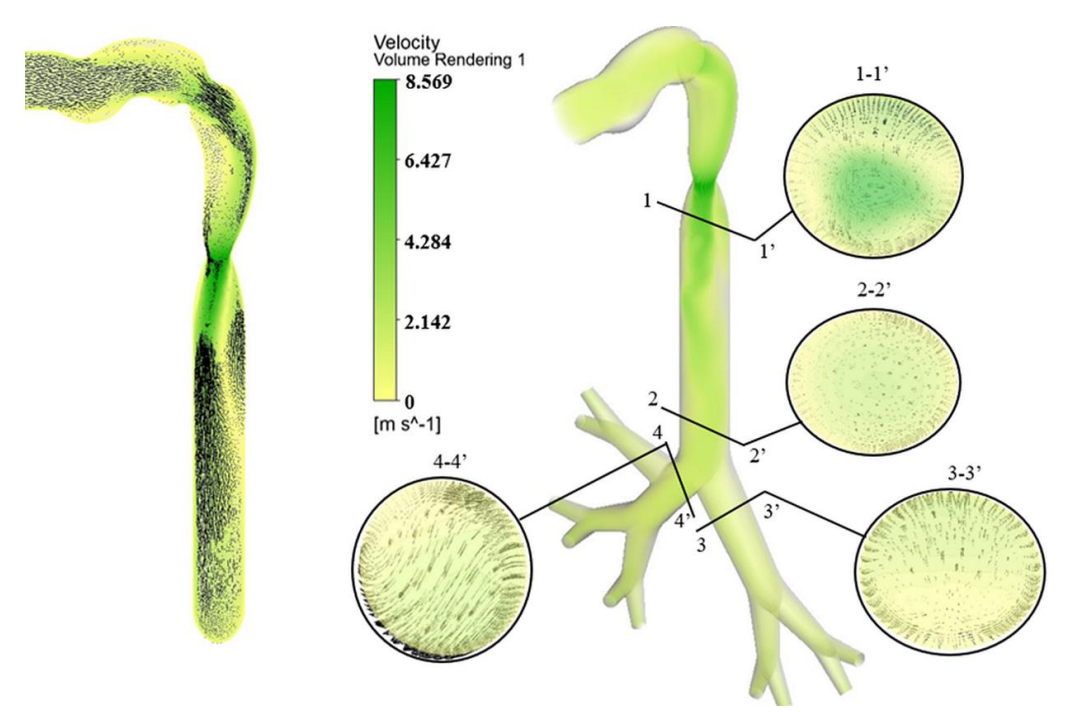


Fig. 6. Calculated velocity fields during peak inhalation (0.991s)

Another characteristic feature is the higher area weighted average velocity in the right bronchial tree. This suggests that the volumetric flow rate of air going into the right lung is larger than the left lung. It is worth noting here that the velocity values obtained the airway are comparable to those obtained in the literature [29,30]. Similar velocity ranges under comparable conditions have been recorded in previous research, indicating consistent behaviour across different research methodologies. This consistency not only confirms the modelling approach used in the current study but also supports the physiological significance of the findings. It is essential to comprehend these velocity profiles as they can impact factors such as particle deposition, resistance and overall airflow efficiency in the respiratory system. This study adds to a more thorough understanding of respiratory mechanics and boosts confidence in the simulation results by aligning with established data.

#### 3.3.2 Exhalation flow fields

The calculated velocity fields at peak exhalation (3.12s) are shown in Figure 7. The flow field once again demonstrates a jet but with its direction reversed. The volume rendering also shows strong axial flow in the glottis-to-mouth section. Multiple recirculatory flows exhibited themselves across all planes. Weak oscillatory flows were observed near the glottal section. Multiple vortices can be seen throughout the respiratory tract as can be seen from the vector plot in Figure 7.

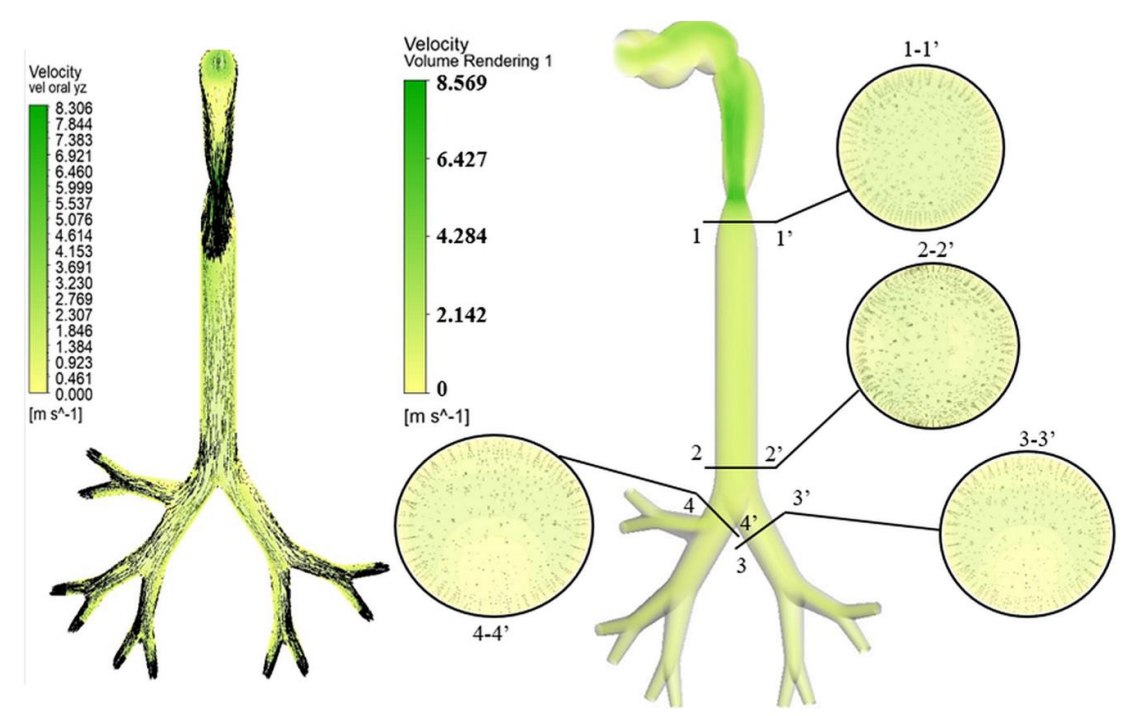


Fig. 7. Calculated velocity fields during peak exhalation (3.451s)

## 3.4 Secondary Flow Vortices

Regions with high vorticity were identified using the Q Criterion. Figure 8 and Figure 9 shows the iso-surfaces developed at  $Q = 100,000 \, s^{-2}$  [31]. Regions with high vorticity in the trachea remained unchanged throughout the cycle. At peak inhalation, small regions with vortex formation are observed near the bifurcation of G0, but as respiration proceeds, these regions move to the higher generations. During exhalation, the length of the secondary flow structures decreased.

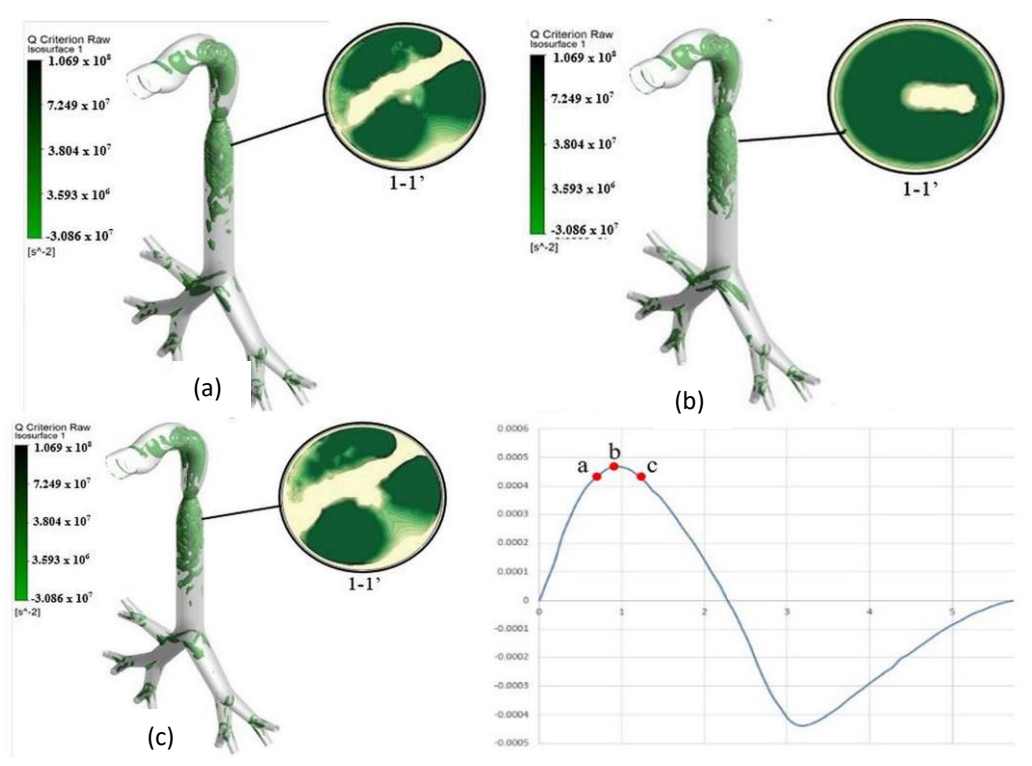


Fig. 8. Iso-surfaces and contours showing Q criterion above 100,000 s-2 (Section 1-1)

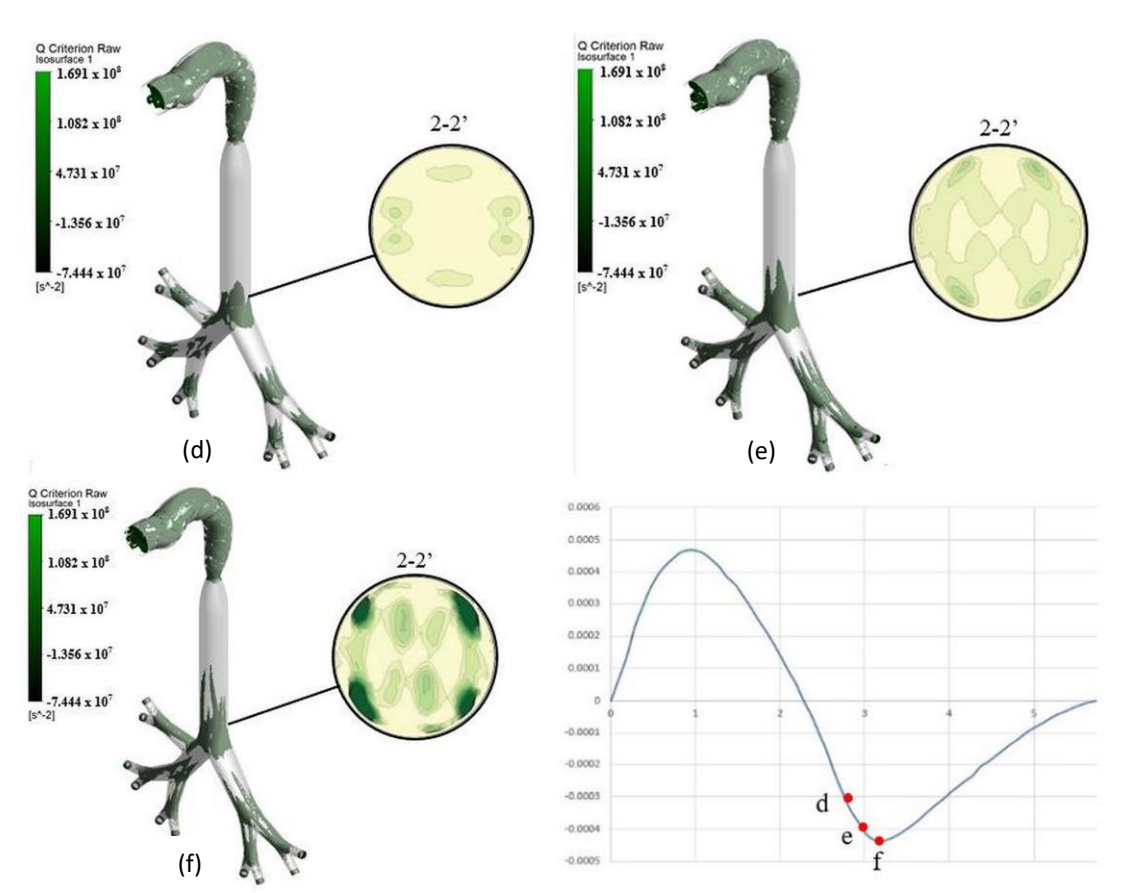
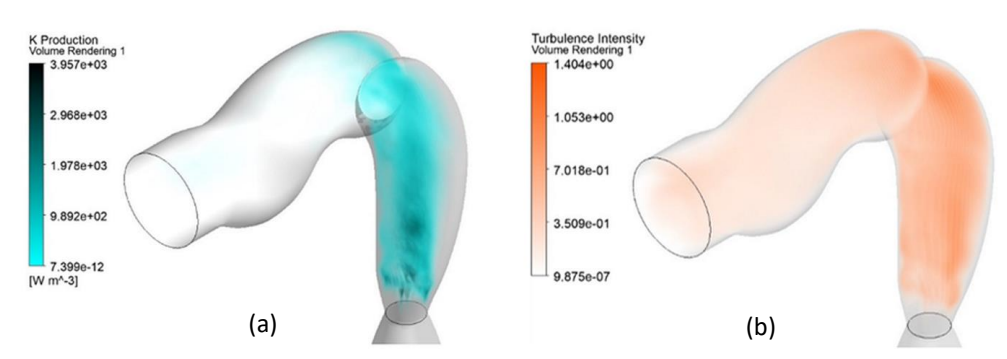


Fig. 9. Iso-surfaces and contours showing Q criterion above 100,000 s-2 (Section 2-2)

At peak inhalation contours at Plane 1-1' showed two areas with recirculatory flows near the left side and a smaller region along the right side. At peak exhalation small regions with recirculation were observed near the bifurcation of the trachea.

#### 3.5 Turbulence Intensity and k Production

Literature reports the presence of turbulent regions of flow in the respiratory tract [10,32] so to corroborate the model a second simulation was setup with the k- $\Omega$  turbulence model switched on. Regions with turbulence were identified by looking at the values of k production and Turbulence intensity. Results showed regions with significant amounts of k production and turbulent intensity in the oral cavity and oropharynx during peak exhalation (Figure 10).



**Fig. 10.** Volume rendering showing (a) k production (b) Turbulence intensity during peak exhalation

During Inhalation, the areas exhibiting higher turbulence were mainly in the tracheal and lower generations. This turbulence is necessary to allow easier gas exchange. **Error! Reference source not found.** shows a volumetric rendering of turbulent areas during inhalation.

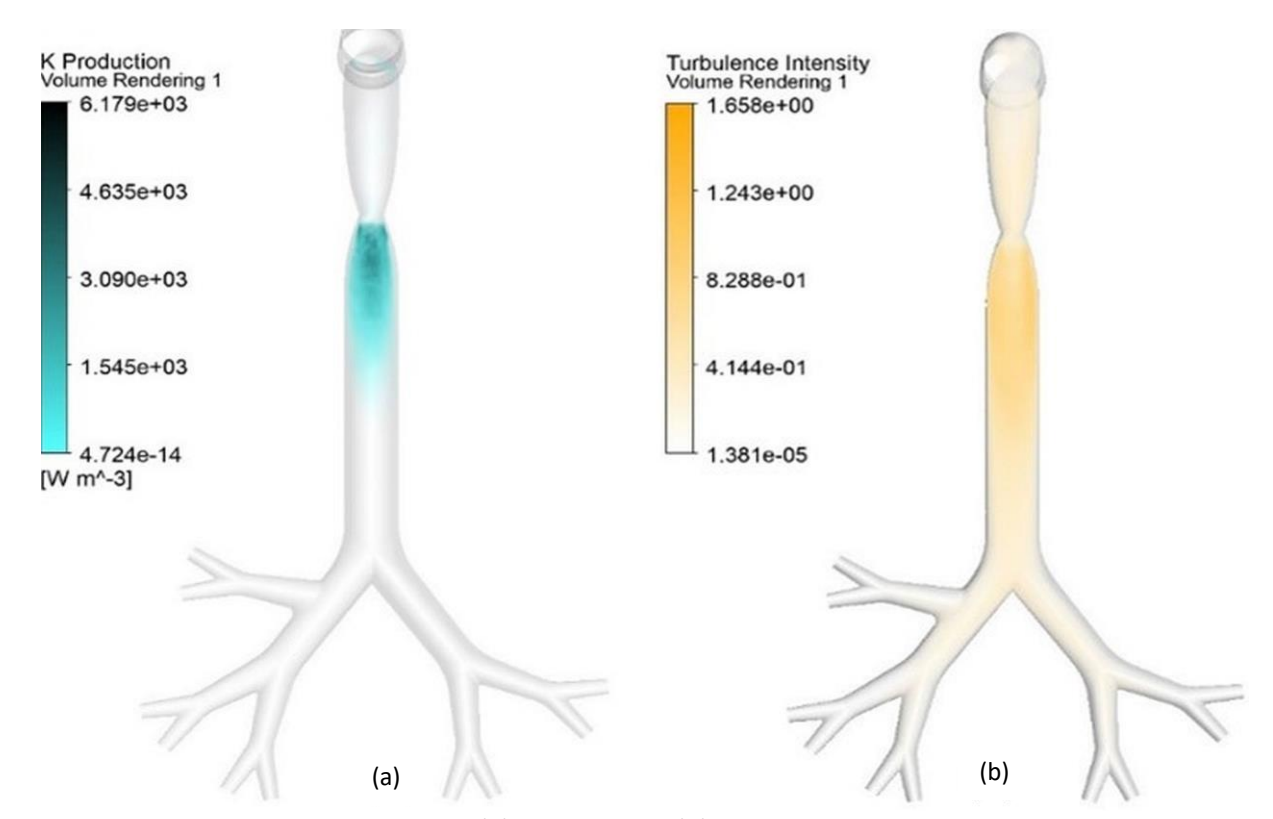


Fig. 11. Volume rendering showing (a) k production (b) Turbulence intensity during peak inhalation

## 3.6 Particle Analysis

Most pharmaceutical aerosol drug inhalers release a metered amount of drug (depending on the weight and age of the patient) when activated. In this case, the drug particles being considered were a formulation of Formoterol Fumerate Dihydrate IP and Budesonide IP [22]. The particle size considered was of  $5\mu m$ . A total of 1161 particles were injected every time step for a duration of 1s from the start of the cycle.

#### 3.6.1 Deposition efficiency

Deposition efficiency (DE) can be defined as the number of particles deposited divided by the total number of particles injected into the domain, also shown in Eq. (8). A higher DE indicates a higher number of particles were trapped in that area Numerically.

Deposition Efficiency 
$$\% = \frac{No.of\ particles\ deposited}{Total\ no.of\ particles\ injected} \times 100$$
 (8)

Figure 12 shows the region-wise Deposition efficiency during one cycle of inhalation. DE comparison shows that the oral cavity region has the highest deposition efficiency of 7.32% and trachea having the least of 0.4% with the overall deposition efficiency being 9.078%. Lower deposition efficiency of drug particles in upper airways is desirable as this indicates the successful transport of the drug to the lower alveolar sacs and the subsequent absorption of it.

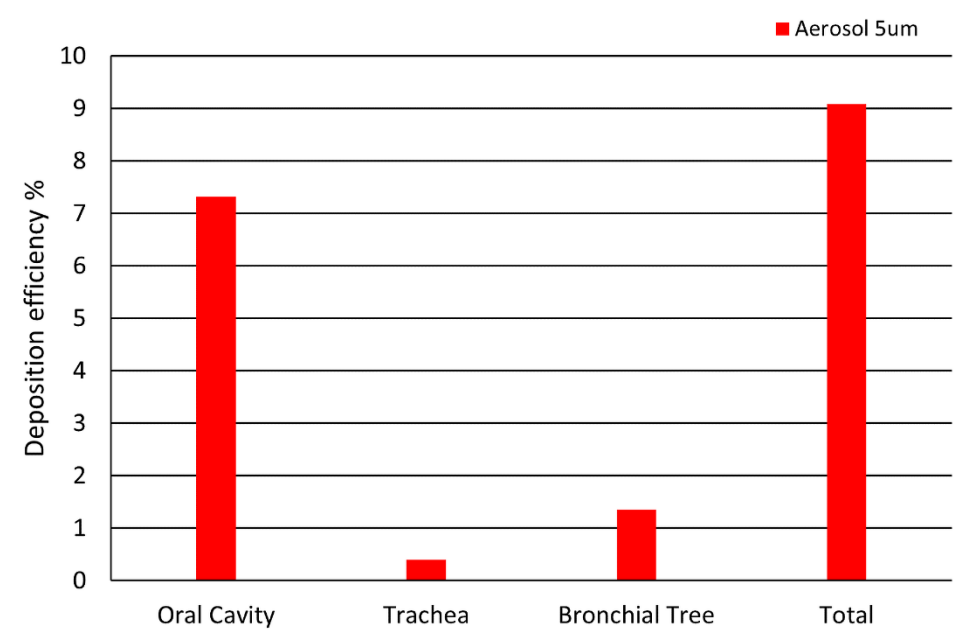


Fig. 12. Region-wise deposition efficiency of aerosol particles

These findings can enhance treatment results for individuals suffering from respiratory issues such as asthma, COPD and cystic fibrosis by optimizing the delivery of medication to the alveolar sacs. This optimization could allow for lower overall medication doses, which may reduce side effects and increase patient compliance. Additionally, the insights can inform the creation of tailored inhalation treatments that consider the unique airway structures and breathing patterns of each patient, ensuring they receive the most effective therapy. The research could further contribute to the design of aerosol particles with specific aerodynamic characteristics to improve targeted delivery, ultimately making inhalation therapies more efficient and user-friendly for patients.

#### 3.6.2 Particle mass concentration

Figure 13 shows the variation of the particle concentration on the walls of the tract as inhalation progresses. It can be seen that during early stages of inhalation the particles are primarily deposited in the oropharynx region but as inhalation progresses the posterior side of the trachea becomes a hotspot. In the bronchial tree the particles are deposited extensively at the bifurcations these are regions where extensive secondary flow structures exist.

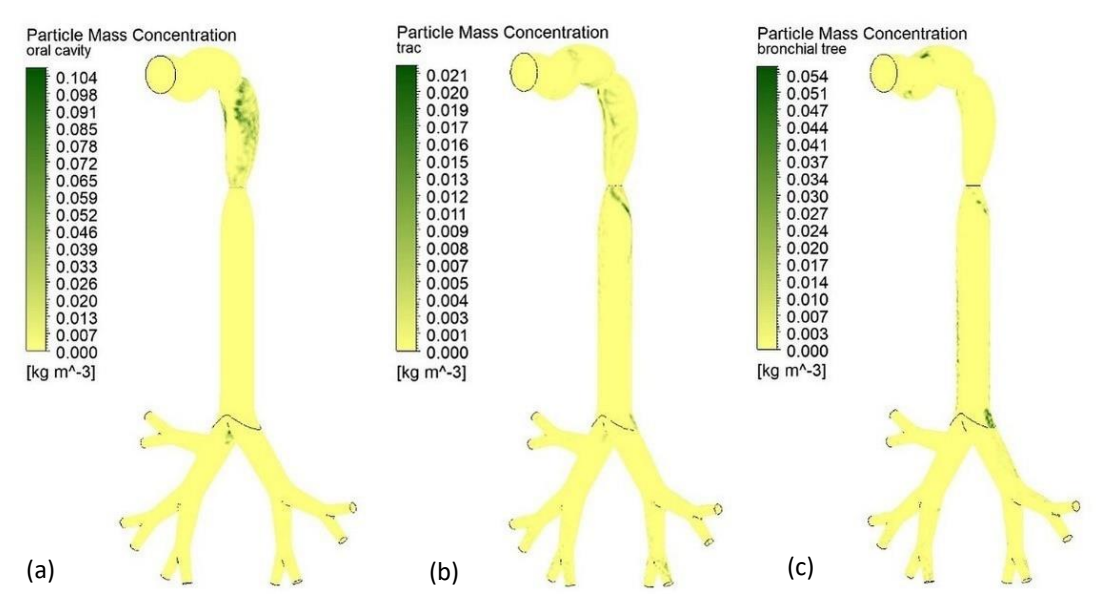


Fig. 13. Particle mass concentration on tract walls at (a) 0.45s (b) 0.99s (c) 1.8s

## 3.7 Limitations of Present Work

The study overlooked the dynamic behaviour of aerosol particles, particularly their tendency to break up when exposed to airflow and collisions. This fragmentation process is crucial as it affects particle size and their deposition efficiency in the respiratory tract, which is vital for inhalation exposure studies. Ignoring particle breakup could compromise the study's accuracy by not fully representing aerosol behaviour, potentially skewing risk assessments and protective measures development. Accurate dosimetry, considering aerosol dynamics like particle breakup, is essential for reliable results and effective strategies against inhalation hazards.

## 4. Conclusions

Idealized human airway model was generated based on the findings from the literature. The airflow patterns were visualized through a simplified model of the human respiratory system using 3D CFD simulations. Axial and secondary flows were seen throughout, with a strong non-axisymmetric axial flow in the upper trachea during inhalation and a reversed laryngeal jet during exhalation. Turbulent kinetic energy was generated in the oropharynx and oral cavity regions, aiding in heat and moisture exchange and facilitating gas exchange in higher generations. Pressure analysis indicated a presence of a global pressure gradient, the higher regions of the respiratory tract on average had higher pressure values throughout inhalation. This pressure gradient is primarily responsible for driving flow into the lower generations and any disruption can hamper normal breathing.

The study of how effectively drug particles deposit in the respiratory system reveals that many reach the deeper parts, like the alveolar sacs, enhancing the therapeutic impact of inhaled medications. This happens as a significant amount of these particles bypass the higher airways, which is beneficial for treatment efficacy. However, a considerable number of particles also end up in the oropharynx and glottal region due to the turbulent airflow in the upper respiratory tract. This turbulence increases the chance of particles getting trapped in these areas, potentially lowering the dose that ultimately reaches the lower airways and alveoli. In the complex structure of the bronchial tree, particle deposition mainly occurs at the bronchi and bronchioles' bifurcations, where airways

split. This phenomenon is attributed to flow separation, leading to low-velocity areas and recirculation zones favourable for particle capture. Understanding how airflow and particle dynamics interact at these bifurcations is key to optimizing respiratory drug delivery. It helps in designing drug formulations and devices that improve particle deposition efficiency in targeted lung areas, ensuring fewer particles are lost and more reach the desired locations in the lungs.

The key findings of this work are summarized below:

- i. The oral cavity and oropharynx regions have the highest mean pressure and particle deposition efficiency, while the posterior side of the trachea becomes increasingly significant for particle deposition as inhalation continues.
- ii. Weak oscillatory flows near the glottal section and multiple vortices throughout the respiratory tract contribute to the distribution and deposition of particles.
- iii. Areas of higher turbulence during inhalation are primarily observed in the tracheal region and lower generations of the respiratory tract, affecting the overall distribution of inhaled substances.

### Acknowledgement

The authors would like to thank the Department of Mechanical & Industrial Engineering, Manipal Institute of Technology, Manipal Academy, Manipal, India and the Department of Aerospace Engineering, Universiti Putra Malaysia, Malaysia, for the computing resources provided to carry out this work.

#### References

- [1] World Health Organization. "Air pollution." World Health Organization, (2023). <a href="https://www.who.int/health-topics/air-pollution#tab=tab">https://www.who.int/health-topics/air-pollution#tab=tab</a> 1
- [2] World Health Organization. "Household air pollution." World Health Organization, (2023) https://www.who.int/news-room/fact-sheets/detail/household-air-pollution-and-health
- [3] Stylianou, Fotos S., Josué Sznitman and Stavros C. Kassinos. "Direct numerical simulation of particle laden flow in a human airway bifurcation model." *International Journal of Heat and Fluid Flow* 61 (2016): 677-710. https://doi.org/10.1016/j.ijheatfluidflow.2016.07.013
- [4] Chen, Zixi, Shamini Parameswaran, Yingying Hu, Zhaoming He, Rishi Raj and Siva Parameswaran. "Numerical simulations of high-frequency respiratory flows in 2D and 3D lung bifurcation models." *International Journal for Computational Methods in Engineering Science and Mechanics* 15, no. 4 (2014): 337-344. https://doi.org/10.1080/15502287.2014.904454
- [5] Yanagita, Yoshiki, Kaishan Feng, Yuko Miyamura, Adi Azriff Basri, Mohammad Zuber, Siti Rohani, Abdul Aziz, Kamarul Arifin Ahmad and Masaaki Tamagawa. "Evaluation of Virus Concentration Analysis in the Airway by CFD." Journal of Advanced Research in Numerical Heat Transfer 13, no. 1 (2023): 96-105. https://doi.org/10.37934/arnht.13.1.96105
- [6] Zuber, Mohammad, Kamarul Arifin Ahmad, SM Abdul Khader, R. Balakrishnan, Sharath Honnani, Sana Althaf Hussain and A. B. V. Barboza. "Effect of Septum Deviation on the Airflow Distribution for a Patient Specific Model using Numerical Methods." *Journal of Advanced Research in Numerical Heat Transfer* 14, no. 1 (2023): 49-57. https://doi.org/10.37934/arnht.14.1.4957
- [7] Napoli, Nicholas J., Victoria R. Rodrigues and Paul W. Davenport. "Characterizing and modeling breathing dynamics: Flow rate, rhythm, period and frequency." Frontiers in Physiology 12 (2022): 772295. https://doi.org/10.3389/fphys.2021.772295
- [8] Weibel, E. R. "Morphometry of the human lung: the state of the art after two decades." *Bulletin europeen de physiopathologie respiratoire* 15, no. 5 (1979): 999-1013.
- [9] Islam, Mohammad S., Suvash C. Saha, Tevfik Gemci, Ian A. Yang, Emilie Sauret and YuanTong Gu. "Polydisperse microparticle transport and deposition to the terminal bronchioles in a heterogeneous vasculature tree." *Scientific reports* 8, no. 1 (2018): 16387. https://doi.org/10.1038/s41598-018-34804-x

- [10] Jing, Hao, Haiwen Ge, Hui Tang, Ali Farnoud, Mohammad Saidul Islam, Li Wang, Chenglei Wang and Xinguang Cui. "Assessing airflow unsteadiness in the human respiratory tract under different expiration conditions." *Journal of Biomechanics* 162 (2024): 111910. <a href="https://doi.org/10.1016/j.jbiomech.2023.111910">https://doi.org/10.1016/j.jbiomech.2023.111910</a>
- [11] Ma, Ruiping, Zhenzhen Hu, Lin Tian, Guoxi Zheng, Yusheng Wang, Xiaole Chen, Miao Lou *et al.*, "Numerical and experimental analysis of pollen inhalation exposure in nasal airways following various middle turbinectomy." *Science of the Total Environment* 907 (2024): 168156. https://doi.org/10.1016/j.scitotenv.2023.168156
- [12] Yatim, Ardiyansyah Saad and Elang Pramudya Wijaya. "Air Quality Improvement in COVID-19 Pandemic: Numerical Study of ventilation system in a classroom." *CFD Letters* 15, no. 1 (2023): 26-38. https://doi.org/10.37934/cfdl.15.1.2638
- [13] Khairulfuaad, Riyadhthusollehan, Norzelawati Asmuin, Juntakan Taweekun, Azizan Ismail and Nabil Izzuddin Shahhidan. "CFD Analysis for Valve-Holding Camber Permanent Inhaler Spacer (AerospaAcer) with Different Valves." *CFD Letters* 16, no. 6 (2024): 53-67. <a href="https://doi.org/10.37934/cfdl.16.6.5367">https://doi.org/10.37934/cfdl.16.6.5367</a>
- [14] Feng, Kaishan, Yoshiki Yanagita, Yuko Miyamura, Adi Azriff Basri, Mohammad Zuber, Siti Rohani, Kamarul Arifin Ahmad and Masaaki Tamagawa. "CFD Analysis of Indoor Ventilation for Airborne Virus Infection." *Journal of Advanced Research in Numerical Heat Transfer* 14, no. 1 (2023): 1-16. https://doi.org/10.37934/arnht.14.1.116
- [15] ICRP (International Commission on Radiological Protection). "Human respiratory tract model for radiological protection." *A Report of a Task Group the International Commission on Radiological Protection Ann ICRP 24 (1–3)* (1994). https://doi.org/10.1016/0146-6453(94)90018-3
- [16] Horsfield, Keith, Gladys Dart, Dan E. Olson, Giles F. Filley and Gordon Cumming. "Models of the human bronchial tree." *Journal of applied physiology* 31, no. 2 (1971): 207-217. https://doi.org/10.1152/jappl.1971.31.2.207
- [17] Augusto, L. L. X., G. C. Lopes and J. A. S. Gonçalves. "A CFD study of deposition of pharmaceutical aerosols under different respiratory conditions." *Brazilian Journal of Chemical Engineering* 33 (2016): 549-558. <a href="https://doi.org/10.1590/0104-6632.20160333s20150100">https://doi.org/10.1590/0104-6632.20160333s20150100</a>
- [18] Srivastav, Vivek Kumar, Akshoy R. Paul and Anuj Jain. "Capturing the wall turbulence in CFD simulation of human respiratory tract." *Mathematics and computers in simulation* 160 (2019): 23-38. https://doi.org/10.1016/j.matcom.2018.11.019
- [19] Larrabee, M. G. and G. C. Knowlton. "Excitation and inhibition of phrenic motoneurones by inflation of the lungs." *American Journal of Physiology-Legacy Content* 147, no. 1 (1946): 90-99. <a href="https://doi.org/10.1152/ajplegacy.1946.147.1.90">https://doi.org/10.1152/ajplegacy.1946.147.1.90</a>
- [20] Zechman, Fred, Frank Gregory Hall and Wayland E. Hull. "Effects of graded resistance to tracheal air flow in man." *Journal of applied physiology* 10, no. 3 (1957): 356-362. https://doi.org/10.1152/jappl.1957.10.3.356
- [21] Chen, Xiaole, Wenqi Zhong, Baobin Sun, Baosheng Jin and Xianguang Zhou. "Study on gas/solid flow in an obstructed pulmonary airway with transient flow based on CFD–DPM approach." *Powder technology* 217 (2012): 252-260. https://doi.org/10.1016/j.powtec.2011.10.034
- [22] Nirale, N. M., M. S. Nagarsenker, S. B. Mendon, R. Chanagare, A. Katkurwar and V. Lugade. "Comparison of aerosol formulations of formoterol fumarate and budesonide." *Indian Journal of Pharmaceutical Sciences* 73, no. 3 (2011): 282.
- [23] Amaral, Simone Simões, João Andrade de Carvalho Jr, Maria Angélica Martins Costa and Cleverson Pinheiro. "An overview of particulate matter measurement instruments." *Atmosphere* 6, no. 9 (2015): 1327-1345. <a href="https://doi.org/10.3390/atmos6091327">https://doi.org/10.3390/atmos6091327</a>
- [24] Kleinstreuer, C. and Z. Zhang. "Airflow and particle transport in the human respiratory system." *Annual review of fluid mechanics* 42, no. 1 (2010): 301-334. https://doi.org/10.1146/annurev-fluid-121108-145453
- [25] Farooq, Umar, Hafiz Hamza Riaz, Adnan Munir, Ming Zhao, Ammar Tariq and Mohammad S. Islam. "Application of heliox for optimized drug delivery through respiratory tract." *Physics of Fluids* 35, no. 10 (2023). https://doi.org/10.1063/5.0169934
- [26] Gemci, T., Valery Ponyavin, Y. Chen, H. Chen and R. Collins. "Computational model of airflow in upper 17 generations of human respiratory tract." *Journal of Biomechanics* 41, no. 9 (2008): 2047-2054. https://doi.org/10.1016/j.jbiomech.2007.12.019
- [27] Islam, Mohammad S., Puchanee Larpruenrudee, Suvash C. Saha, Oveis Pourmehran, Akshoy Ranjan Paul, Tevfik Gemci, Richard Collins, Gunther Paul and Yuantong Gu. "How severe acute respiratory syndrome coronavirus-2 aerosol propagates through the age-specific upper airways." *Physics of Fluids* 33, no. 8 (2021). https://doi.org/10.1063/5.0061627
- [28] Islam, Mohammad S., Puchanee Larpruenrudee, Sheikh I. Hossain, Mohammad Rahimi-Gorji, Yuantong Gu, Suvash C. Saha and Gunther Paul. "Polydisperse aerosol transport and deposition in upper airways of age-specific lung." *International journal of environmental research and public health* 18, no. 12 (2021): 6239. https://doi.org/10.3390/ijerph18126239

- [29] Rahman, Md M., Ming Zhao, Mohammad S. Islam, Kejun Dong and Suvash C. Saha. "Numerical study of nanoscale and microscale particle transport in realistic lung models with and without stenosis." *International Journal of Multiphase Flow* 145 (2021): 103842. <a href="https://doi.org/10.1016/j.ijmultiphaseflow.2021.103842">https://doi.org/10.1016/j.ijmultiphaseflow.2021.103842</a>
- [30] Rahman, Md M., Ming Zhao, Mohammad S. Islam, Kejun Dong and Suvash C. Saha. "Aerosol particle transport and deposition in upper and lower airways of infant, child and adult human lungs." *Atmosphere* 12, no. 11 (2021): 1402. https://doi.org/10.3390/atmos12111402
- [31] Gaddam, Manikantam G. and Arvind Santhanakrishnan. "Effects of varying inhalation duration and respiratory rate on human airway flow." *Fluids* 6, no. 6 (2021): 221. <a href="https://doi.org/10.3390/fluids6060221">https://doi.org/10.3390/fluids6060221</a>
- [32] Zhang, Zhe and Clement Kleinstreuer. "Laminar-to-turbulent fluid–nanoparticle dynamics simulations: Model comparisons and nanoparticle-deposition applications." *International Journal for Numerical Methods in Biomedical Engineering* 27, no. 12 (2011): 1930-1950. https://doi.org/10.1002/cnm.1447